Boosting Thermoelectric Power Factor of Carbon Nanotube Networks with Excluded Volume by Co-Embedded Microparticles

Oluwasegun Isaac Akinboye, Yu Zhang, Vamsi Krishna Reddy Kondapalli, Fan Yang, Viktor Mandrolko, Mykola Isaiev, Gilles Pernot, Vesselin Shanov, Yue Wu, Je-Hyeong Bahk

Boosting Thermoelectric Power Factor of Carbon Nanotube Networks with Excluded Volume by Co-embedded Microparticles

Oluwasegun Isaac Akinboye[1], Yu Zhang[1], Vamsi Krishna Reddy Kondapalli[1], Fan Yang[2], Viktor Mandrolko[4], Mykola Isaiev[4], Gilles Pernot[4], Vesselin Shanov[3], Yue Wu[2], and Je-Hyeong Bahk[1*]

[1]Department of Mechanical and Materials Engineering, University of Cincinnati, Cincinnati, OH 45221, USA

[2]Department of Chemical and Biological Engineering, Iowa State University, Ames, IA 50011, USA

[3]Department of Chemical and Environmental Engineering, University of Cincinnati, Cincinnati, OH 45221, USA

[4] Université de Lorraine, CNRS, LEMTA, F-54000, Nancy, France

*Email: bahkjg@ucmail.uc.edu

ABSTRACT

Carbon nanotube (CNTs) networks embedded in a polymer matrix have been extensively studied as a flexible thermoelectric transport medium over the recent years. However, their power factor has been largely limited by the relatively inefficient tunneling transport at junctions between CNTs and the low-density conducting channels throughout the networks. This work demonstrates that significant power factor enhancements can be achieved by adding electrically insulating microscale particles in three-dimensional CNT networks embedded in the polymer matrix. When silica particles of a few μm diameters were co-embedded in single-walled CNT (SWCNT)-polydimethylsiloxane (PDMS) composites, both the electrical conductivity and the Seebeck coefficient were simultaneously enhanced, thereby boosting the power factor by more than a factor of six. We found that the silica microparticles excluded a large volume of the composite from the access of CNTs and caused CNT networks to form around them with the polymer as a binder, resulting in improved network connectivity and alignment of CNTs. Our theoretical calculations based on junction tunneling transport for three-dimensional CNT networks show that the significant power factor enhancement can be attributed to the enhanced tunneling with reduced junction distance between CNTs. Additional power factor enhancement by a factor of three was achieved by sample compression, which further reduced the mean junction distance to enhance tunneling, but also reduced the geometric factor at the same time, limiting the enhancement of electrical conductivity.

KEYWORDS: carbon nanotube networks, thermoelectric transport, silica microparticles, flexible thermoelectric material, power factor enhancement

1. Introduction

Research on thermoelectric (TE) materials has accelerated in recent years due to the world-wide efforts for low-grade waste heat recovery and wearable body-heat harvesting.[1-3] The performance of a TE material is evaluated using the unitless figure-of-merit $zT = S^2\sigma T/\kappa$, which is dependent on the Seebeck coefficient (S), electrical conductivity (σ), and thermal conductivity (κ).[3] T is the absolute temperature. The numerator part ($S^2\sigma$) in zT is called the power factor (PF), which determines the power output of a TE device for a given temperature difference. PF is a material property determined by charge carrier transport in the material. The trade-off relationship between S, σ, and κ is a fundamental issue that has hampered further enhancement of TE materials performance.[4-5]

Due to their excellent chemical and thermal stability and outstanding electrical and mechanical properties, carbon nanotubes (CNTs) are frequently utilized as fillers in nanocomposites and have thus emerged as a promising candidate for developing novel flexible TE devices. [6-8] In particular, single-walled CNTs (SWCNTs) have been extensively studied to utilize their low dimensionality with sharp features in the electronic density of states for enhanced TE properties. [4,9] Recently, many reports explored the TE performances of individual CNTs [10-12] and their hybrid composites with polymers [6,13-16]. In their composites with polymers, CNTs create intimate networks to provide electric percolation channels and thus reasonably high power factors, while the polymer matrix primarily offers low thermal conductivities. However, their zT values are still much lower (< 0.1) than those of the state-of-the-art inorganic TE materials (zT ~1). Networks made of only metallic SWCNTs exhibiting zero bandgaps have shown much lower Seebeck coefficients (< 20 μV/K) compared to those of semiconducting ones (> 150 μV/K).[17] Neat SWCNTs typically consist of mixed semiconducting and metallic ones. They typically showed Seebeck coefficients in the range of 40 ~ 90 μV/K in both p-type and n-type regimes. [13-16,17-18] Recently, Avery et al. [7] reported a very high Seebeck coefficient greater than 400 μV/K for semiconducting (s-) SWCNT networks, but at relatively low electrical conductivities due to the trade-off between the two properties. High power factors greater than 200 μW m^{-1} K^{-1} were obtained with highly doped SWCNTs to achieve high electrical conductivities with sacrifice in the

Seebeck coefficient. MacLeod et al. [19] further optimized the doping of s-SWCNTs to achieve very high power factors ~ 700 μW m^{-1} K^{-1} in both p-type and n-type regimes.

Despite these exciting recent studies, the fundamental TE transport through CNT networks has not been fully understood. In CNT networks, charge carriers flow internally along a CNT and then pass through the junction between CNTs by tunneling to reach the next CNT. This process is repeated until the charge carriers reach the other end of the sample. Hence, the Seebeck coefficient as well as the electrical conductivity are basically affected by both the internal transport along CNTs and the junction tunneling. The net Seebeck coefficient is then the weighted average between the Seebeck coefficients from the internal transport (S_{CNT}) and across the junction (S_{junc}) with weighting factors of the fraction of temperature difference applied across them, such that

$$S = \frac{\Delta T_{\mathrm{CNT}}}{\Delta T} S_{\mathrm{CNT}} + \frac{\Delta T_{\mathrm{junc}}}{\Delta T} S_{\mathrm{junc}} \qquad (1)$$

Statz et al. [20] argued that the Seebeck coefficient is primarily determined by the internal Seebeck coefficient, i.e., $S \sim S_{\mathrm{CNT}}$, in their dense CNT films because the junctions are mostly orthogonal to the temperature gradients in dense CNT network films, so that $\Delta T_{\mathrm{junc}} \sim 0$. This may be possible when CNTs create quasi-two-dimensional networks in a thin film with no other significant material components or matrix involved in the networks as illustrated in Fig. 1(a). Due to the high aspect ratio of CNTs, they tend to be stacked parallel to the substrate, and then the junctions, which are the shortest distance points between neighboring CNTs, are created vertically in the direction normal to the in-plane temperature gradients. In this case, the temperature difference across the junctions can be negligibly small, and the in-plane Seebeck coefficient will be determined primarily by the internal Seebeck coefficient of CNTs as pointed out by Statz et al. [20]. It is noteworthy that the electrical conductivity will still be influenced by the junction tunneling in the quasi-2D networks.

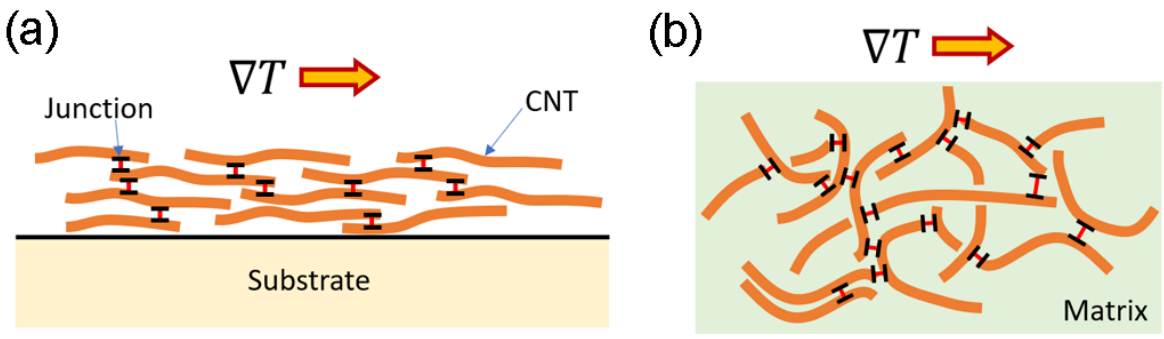

Figure 1. Illustration of two different CNT network formations: (a) CNTs deposited on a substrate without a matrix to create quasi-two-dimensional, planar networks, and (b) CNTs embedded in a thick matrix to form three-dimensional networks with random orientation. In (a), junctions are formed in the direction normal to the temperature gradients applied in-plane, while they are formed in random orientation in (b). The in-plane Seebeck coefficient is primarily determined by the internal transport along CNTs in (a), while it is determined by the junction transport in (b).

On the other hand, CNTs randomly dispersed in a thick matrix can create three-dimensional networks as shown in Fig. 1(b), where the junctions are formed with random orientation in all three dimensions. Significant temperature differences can be applied across the junctions that are in the direction of temperature gradients in this case. The divided temperature differences in Eq. (1) are determined in proportion to the thermal conductances of the individual segments along the path. Studies based on molecular dynamic and atomistic Green's function simulations showed that the thermal conductance at the cross-bar junction between two CNTs is as low as ~50 pW/K, which is two orders of magnitude lower than those of individual CNTs (~ 5,000 pW/K for 1 μm effective length in the direction of temperature gradients and ~ 1 nm diameter with 3,000 W/mK thermal conductivity).[21-23] The resulting upper bounds of thermal conductivity for CNT networks are found to be only a few W/mK [22], despite the extremely high thermal conductivity of individual CNTs (3,000 W/mK) because of the extremely low thermal conductance at junctions. These results indicate that the temperature difference across junctions can be about two orders of magnitude greater than those along individual CNTs, i.e., $\Delta T_{\text{junc}} \gg \Delta T_{\text{CNT}}$, so that the Seebeck coefficients of three-dimensional CNT networks are predominantly determined by the junction tunneling according to Eq. (1).

Our previous work on SWCNT networks embedded in ~1-mm thick polydimethylsiloxane (PDMS) elastomer showed highly isotropic TE properties between in-plane and cross-plane

properties, confirming the formation of three-dimensional CNT networks.[13] Both the Seebeck coefficient and the electrical conductivity were significantly varied with CNT content in the composite, which cannot be explained if the properties were determined by the those of individual CNTs. We employed Landauer theory to calculate the TE properties at the junctions and the variation of the properties with CNT content were successfully explained with decreasing junction distance with increasing CNT content. CNT composites with polyaniline (PANI) [24] and polypyrrole [25] also showed similar variations of the Seebeck coefficient and electrical conductivity with CNT content.

Recently, Park et al. [26] showed that the electrical conductivity of CNT networks could be enhanced by adding microscale particles as secondary fillers. These microparticles (MPs) created excluded volume and pinched CNTs into the narrow space between the microparticles to form denser, better-connected percolation networks of CNTs, resulting in enhanced electrical conductivity. However, the effects of segregated CNT networks by excluded volume on the TE transport, particularly on the Seebeck coefficient, have not been thoroughly investigated. Furthermore, previous investigations have often seen irregular trends in electrical conductivity with a small inclusion of secondary fillers in hybrid CNT composite systems.[27-28]

In this work, we combine experimental and theoretical studies to investigate the effects of silica microparticles co-embedded with CNTs in a polymer matrix on the TE transport properties with broadly varying microparticle content. PDMS is employed as the matrix for this study due to its many advantages, such as solution processability, lightweight, biocompatibility, and low thermal conductivity.[13,29] PDMS also works as an excellent binder between CNTs and silica particles. Silica particles are chosen as the filler material due to their excellent compatibility with CNTs and PDMS for a uniform dispersion and stable network formation.[30] Furthermore, their wide availability and cost-effectiveness make them a practical option for large-scale applications, and their biocompatibility renders the composite along with PDMS suitable for wearable applications, such as body-heat harvesting. Since both PDMS and silica particles are electrically insulating, all the carrier transport occurs through CNT networks. Hence, this material combination provides an excellent model system to study the variation of TE properties exclusively by a modification to CNT networks with microparticles.

2. Experimental Methods

Single-walled carbon nanotubes (SWCNT), silica MPs, PDMS prepolymers, and curing agent are the raw components for the CNT-based polymer composites material development, and chloroform was used as the solvent. Dow Corning supplied commercially available PDMS (Sylgard 184 Silicone Elastomer Base) to synthesize the CNT-based polymer composite. Tuball SWCNTs from Sigma Aldrich with an average diameter of 1.6 nm and a length of > 5 μm was utilized. Silica powders of 1 and 3 μm particle size were bought from Sigma Aldrich. The raw components were all used as received.

For the composite synthesis, it is imperative that the two fillers (SWCNTs and silica MPs) disperse evenly in the PDMS matrix. Despite their comparable structures, poor distribution conditions of these two filler materials in the PMDS matrix can generate opposing or irregular trends in electrical conductivity.[26] Ultrasonication guaranteed uniform mixing and excellent dispersion of entangled CNTs and silica microparticles in PDMS. They were initially disseminated in chloroform using ultrasonic agitation at a frequency of 20 kHz. These processes resulted in the homogenous dispersion conditions of the fillers in PDMS. CNT content was fixed at 10 w.t.%, and PDMS content was varied to accommodate a broad range of silica content from 0 to 60 w.t.% for the study. The resulting samples are free-standing without substrate, and the thicknesses varied from ~ 0.9 to ~ 1.2 mm before compression. Samples were then compressed between two cylindrical rollers 0.5 mm apart to produce 0.5 mm thick compressed samples. More detailed information about the synthesis processes and sample compression is found in Supporting Information (Section 1). Scanning electron microscopy (SEM) (FEI XL30, 15 kV) was used to examine the morphological and structural characteristics of the composites. The samples were also examined using Raman spectroscopy (Renishaw inVia, stimulated by a 514 nm Ar – ion laser with a laser spot size of approximately 1 μm^2 and a lens of 50X).

The thermoelectric properties of the composites were measured using a custom-built set-up at room temperature. A sample of 1.5×1 cm^2 was placed like a bridge between two thermoelectric modules, which created temperature differences across the sample. Two thermocouples were used to measure temperature differences, and the Seebeck voltage was measured using a separate pair of electrodes placed at the same positions that the thermocouples were placed. The electrical conductivity was measured using the van der Pauw method with four edge contacts on the samples. Additionally, the micro-Raman scattering technique was employed for thermal conductivity measurements of the samples. [31] This approach creates thermal perturbation on the sample by

laser heating. From the Raman peak frequency, one can estimate the average temperature in the sample excited by the beam. This allows us to evaluate the thermal conductivity by resolving the inverse heat conduction problem. More information about the thermal conductivity measurement with this technique is available in the Supplementary Information (Section 7).

3. Theoretical Investigation

Since the junction conductance is orders of magnitude smaller than the internal conductance of individual CNTs in both electron and thermal transport regimes, we assume that the junction tunneling is the dominant transport mechanism in determining the effective bulk TE properties, and the transport properties of individual CNTs are negligibly small. For junction tunneling, we employ the Landauer formalism. [32] More details about the transport calculations can be found in our previous work. [13]. In Landauer, the electrical conductance, the Seebeck coefficient, and the electronic thermal conductance of each carrier type are all integral functions of the differential conductance $G'(E)$ with respect to the carrier energy E given, respectively, by

$$G_i = \int_0^\infty G'(E)\, dE \tag{2}$$

$$S_i = \frac{1}{qT} \frac{\int_0^\infty G'(E)(E-E_F)dE}{\int_0^\infty G'(E)dE} \tag{3}$$

$$K_{\mathrm{elec},i} = \frac{2}{hT} \int_0^\infty G'(E)(E-E_F)^2 dE - S_i^2 G_i T \tag{4}$$

where the subscript i is either 'e' for electrons or 'h' for holes. E= 0 at the band edge, and the integral is performed for each band using the unit charge q = -e for the conduction band to represent electrons and q = +e for the valence band to represent holes. E_F is the Fermi level. The differential conductance at a junction is defined as $G'(E) = G_0 \bar{T}(E) M(E) \left(-\frac{\partial f_0}{\partial E}\right)$, where $G_0 = 2e^2/h$ is the quantum of conductance, $\bar{T}(E)$ is the tunneling transmission through the junction ($0 \leq \bar{T}(E) \leq 1$), $M(E)$ is the number of modes, and f_0 is the Fermi-Dirac distribution function. The $\left(-\frac{\partial f_0}{\partial E}\right)$ is a bell-shaped function centered at the Fermi level called the Fermi window, of which the full width half maximum is proportional to the absolute temperature. The Fermi window defines the energy range of carriers that participate in the conduction. In our model, a potential barrier is determined by the material occupying the gap, e.g., the polymer matrix. We assume a square potential for tunneling, which is a good assumption for high tall, thin barriers with very

small voltage across the junction. [33] Assuming a one-dimensional square potential barrier in the tunneling regime, the transmission is known as

$$\bar{T}(E) = \left[1 + \frac{E_B^2 \sinh^2(kd)}{4E(E_B - E)}\right]^{-1} \quad (5)$$

where E_B is the barrier height from the band edge of CNTs, d is the junction distance, and $k = (E_B - E)/(\hbar v_F)$ is the wave vector corresponding to the energy difference between the barrier height and carrier energy. v_F = 8.5 × 10^5 m/s is the Fermi velocity representing the linear dispersion for SWCNTs.

For polymer gaps, the barrier height is determined by the energy difference between the band edges of the CNT and the polymer, i.e., between the conduction band edge of CNT and the LUMO level of the polymer for electrons or between the valence band edge of CNT and the HOMO level of the polymer for holes. Therefore, the barrier height for holes is typically different from that for electrons, i.e., asymmetric barrier heights for two carrier types. Due to the asymmetric barriers, the resulting TE properties in the p-type and n-type regimes can be highly different from each other in the tunneling-limited transport for 3D CNT networks embedded in polymer matrix. However, for quasi-2D CNT networks shown in Fig. 1(a), the TE properties are symmetric between p-type and n-type regimes [20] because they are largely determined by the internal transport along CNTs, where the band structures and the scattering characteristics are fundamentally symmetric.

Since we are using undoped SWCNTs in this work, we expect that the transport is in the bipolar regime, where both electrons and holes are non-negligibly contributing to the net transport. Our SWCNTs show positive Seebeck coefficients due to natural oxidation in air, which makes CNTs slightly p-type. We use the Fermi level as a fitting parameter to fit the experimental data with theory. Due to the slight p-type nature of our SWCNTs, the best fit is found to be the Fermi level at 40 meV below the Dirac point, i.e., $E_F = -40$ meV. In the bipolar transport regime, the total properties are given, respectively, by

$$G = G_e + G_h \quad (6)$$

$$S = \frac{G_e S_e + G_h S_h}{G_e + G_h} \quad (7)$$

$$K_{\text{elec}} = K_{\text{elec},e} + K_{\text{elec},h} + K_{\text{bi}} \quad (8)$$

where K_{bi} is the bipolar thermal conductance given by

$$K_{\mathrm{bi}} = \frac{G_e G_h}{G_e + G_h}(S_h - S_e)^2 T \qquad (9)$$

Fig. 2(a) shows the total Seebeck coefficient as a function of Fermi level spanning the p-type, bipolar, and n-type regimes. Here, we used asymmetric barrier heights for electrons and holes to explain our experimental data: 2 eV for electrons and 2.2 eV for holes. Due to the slightly lower barrier height for electrons, the unipolar electrical conductance of electrons G_e is larger than that of holes G_h at the same energy. Therefore, electrons contribute more to the total Seebeck coefficient given by Eq. (7), where the unipolar electrical conductances are used as weighting factors. As a result, the Seebeck curve is shifted to the left. This is the reason that the total Seebeck coefficient shown in Fig. 2(a) is negative (n-type) at zero Fermi level.

Fig. 2(a) also shows the variation of Seebeck coefficient with junction distance. The junction distance varied from 7 (red) to 10 Å (green) with a step of 0.5 Å. In the unipolar regions at both p-type and n-type sides, the magnitude of Seebeck coefficient increases with increasing junction distance, suggesting the typical trade-off relationship between the Seebeck coefficient and the electrical conductance in these regions as the latter decreases with increasing junction distance. On the other hand, in the p-type bipolar region (the shaded region in gray in the figure), the trend is opposite: the Seebeck coefficient decreases with increasing junction distance. As the junction distance increases, the unipolar conductance of electrons increases much more rapidly than that of holes due to the lower barrier height for electrons, which results in the increased contribution from electrons in the total Seebeck coefficient according to Eq. (7). As a result, the curve is shifted further to the left in the figure, and the magnitude of the Seebeck coefficient is reduced. Since our undoped SWCNTs are within this bipolar region with $E_F = -0.04$ eV, the Seebeck coefficient is expected to increase with decreasing junction distance, which has been observed in our CNT:PDMS composites.[13] Fig. 2(b) clearly shows that both the Seebeck coefficient and the electrical conductance increase with decreasing junction distance in this bipolar regime at E_F = -0.04 eV. Our material system falls in this region, where the reduced junction distance by the inclusion of microparticles simultaneously enhances the Seebeck coefficient and electrical conductivity as will be discussed in the next section.

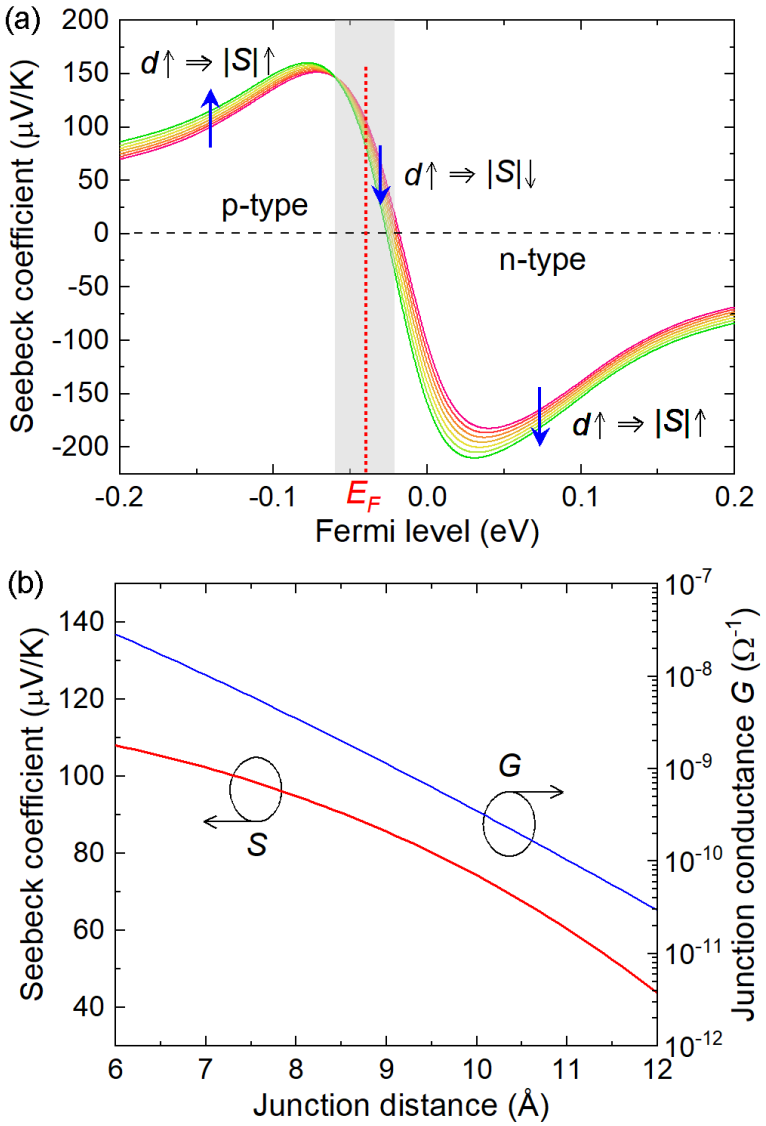

Figure 2. (a) Calculated Seebeck coefficient as a function of Fermi level spanning both p-type and n-type regions including the bipolar region in the middle. The several curves represent the Seebeck coefficient with different junction distance varied from 7 to 10 Å with a step of 0.5 Å (red to green in color). Only in the shaded bipolar region, the Seebeck coefficient decreases with increasing junction distance at a fixed Fermi level. The Fermi level E_F= -0.04 eV for our undoped SWCNTs falls in this region. (b) Calculated Seebeck coefficient and junction conductance as a function of junction distance at the fixed Fermi level E_F= -0.04 eV, showing the simultaneous increase in both properties with decreasing junction distance.

Finally, the electrical conductivity and the thermal conductivity are the product of the junction conductance and the geometric factor, such that

$$\sigma = \alpha G \qquad (10)$$

$$\kappa_{\text{elec}} = \alpha K_{\text{elec}} \quad (11)$$

where the geometric factor α is defined as the ratio of the average number of channels per cross-sectional area, *m*, to the average number of junctions per channel per length, *n*, i.e., $\alpha = \frac{m}{n}$, in the unit of cm^{-1}.[13] The geometric factor indicates the abundance of transport channels and alignment of CNTs toward the transport direction in the networks. For instance, adding more CNTs typically increases the geometric factor until it saturates. Increasing CNT alignment in the transport direction helps increase the geometric factor as well as it reduces the denominator, *n*.

The total thermal conductivity is the sum of the electronic thermal conductivity and the lattice thermal conductivity as in

$$\kappa = \kappa_{\text{elec}} + \kappa_{\text{lat}} \quad (12)$$

In our data fitting with theory, we adjust the junction distance as a fitting parameter to fit the Seebeck coefficient at each silica content. We fixed the Fermi level position during this process as we did not dope or perform any chemical treatments on the CNTs. Once the Seebeck coefficient is fitted with junction distance, we then calculate the electrical conductance G with the determined junction distance and then fit the electrical conductivity with the geometric factor as another fitting parameter using Eq. (10). The electronic thermal conductivity is obtained without additional fitting parameter using Eq. (11). The lattice thermal conductivity is not calculated in this work as it is determined by phonon transport in CNT networks. The total thermal conductivity is experimentally measured.

4. Results and Discussion

4.1. Network Morphology and Raman Spectroscopy

Fig. 3 displays the cross-sectional SEM images of the CNT-silica MP-PDMS composites revealing the morphologies of CNT networks after incorporating with different content of silica MPs. Compared with the sample without silica (as seen in Fig. 3(a)), all other samples showed hair-like CNT bundles connecting the silica particles like bridges. CNTs are also seen closely bound on the surface of silica particles, creating intimate networks on the particle surfaces with PDMS as a binder. The latter proves the creation of excluded volume due to the interactions between silica particles and CNTs. Moreover, it can be observed that as the silica content increased, the excluded volume becomes more apparent and the interconnectivity between the CNT bundles become more

evident, thus contributing to the effective increase in electrical conductivity, which is presented later in this paper.

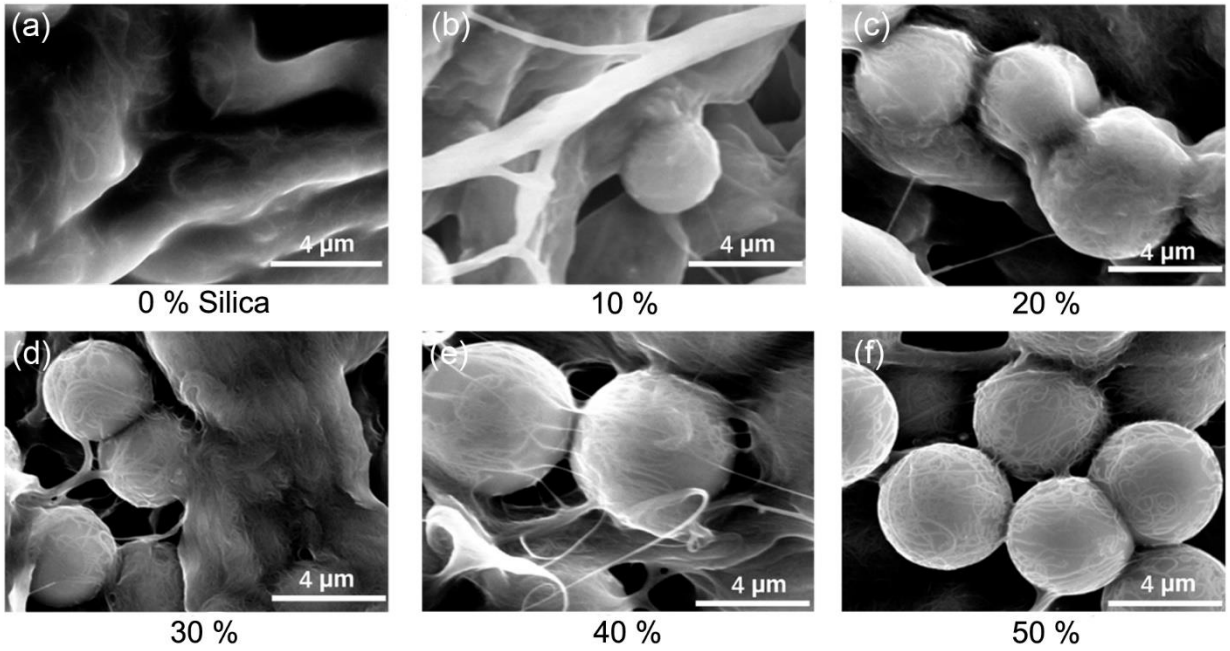

Figure 3. SEM images of SWCNT-silica MP-PDMS composites with varying content of silica particles of 3 µm diameter: (a) no silica, (b) 10 w.t.%, (c) 20 w.t.%, (d) 30 w.t.%, (e) 40 w.t.% and (f) 50 w.t.% silica. SWCNT content kept constant at 10 w.t.% and PDMS content was varied accordingly, i.e., decreasing PDMS w.t.% with increasing silica content.

The clear change of network morphology with the inclusion of silica MPs is illustrated in Fig. 4. By binding CNTs onto silica MPs, more CNTs are utilized to participate in creating conducting channels, thereby increasing the network connectivity and channel density. In terms of tunneling transport modeling, this network morphology change implies the change in junction distance between CNTs as well as in the geometric factor, which will be explained in detail in the next sub-section.

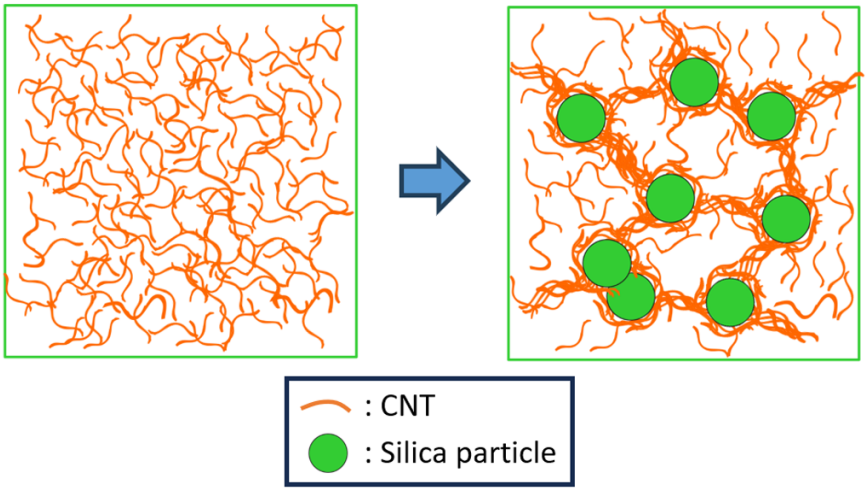

Figure 4. Illustration of CNT network morphology change with the inclusion of silica MPS in CNT- PDMS composites. CNTs are closely bound on the surface of silica particles with PDMS as a binder. CNT bundles connect the sub-networks like a bridge between neighboring silica particles to complete transport pathways throughout the sample.

The SEM images in Fig. 3 highlight the uniform distribution of the CNTs and their bundles around silica particles. Still, these images cannot show the structural changes in the CNT bundles and their respective junctions due to the applied stress. Raman Spectroscopy was used to evaluate the changes, where a 514 nm laser with a spot size of 1 μm^2 and lens of 50X was utilized. The Raman spectra of the CNT-based PDMS composites are highly uniform across the surface, highlighting the high quality of the CNTs used in this work. Irrespective of the composition of the composites, all the spectra featured the signature peaks of CNT; RBM, D, G^-, $G^{+,}$ and 2D peaks. Raman spectra of the SWCNT used in the composite is shown in Fig. 5(a) and the normalized Raman spectra of composites with different silica w.t.% are shown in Fig. 5(b). Peak analysis was performed using VOIGT (convolution of Gaussian and Lorentzian) peak fitting [34] and the G^+ peak positions were extracted and plotted as described in detail elsewhere.[35] A comparison of the G^+ peak position of pristine CNT, compressed CNT, and CNT + PDMS composite with other CNT-based polymer composites with different w.t.% of 3 µm silica was shown in Supporting Information (Section 4)**.** This clarifies that neither the addition of 3 µm silica, PDMS nor compression of freely stacked CNT powder induced any strain in the CNTs as per the G^+ peak positions.

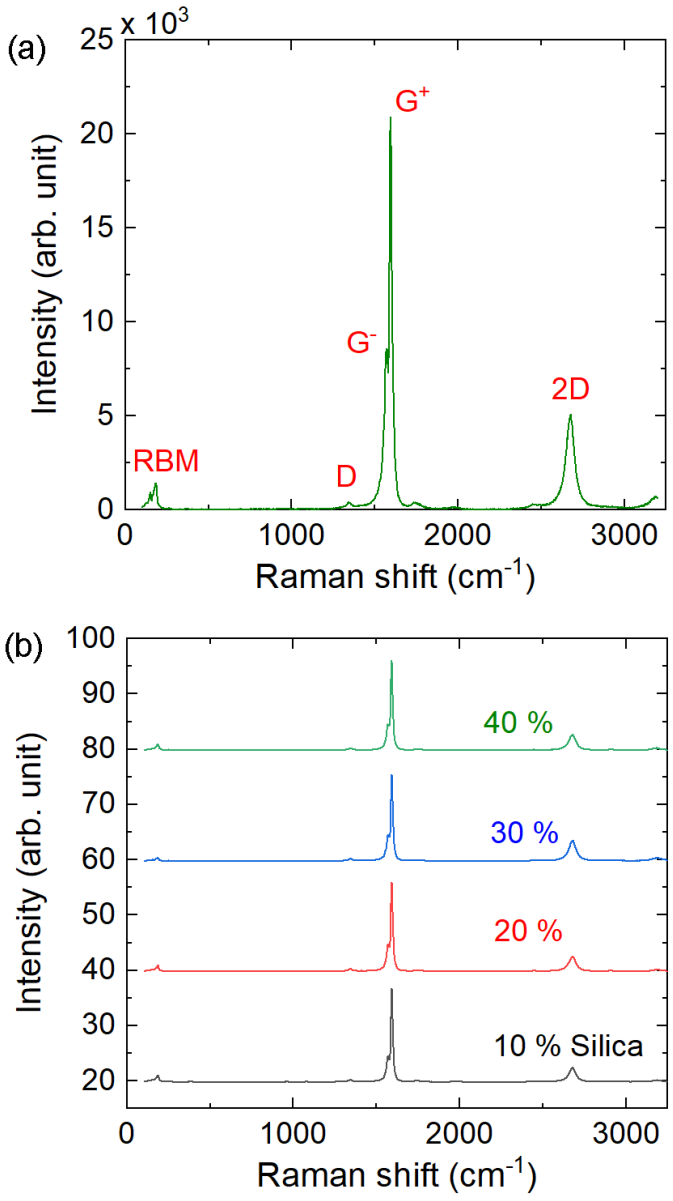

Figure 5. Raman spectra of (a) SWCNTs used in the CNT networks and (b) CNT-silica-PDMS composites with 1 um silica co-embedded in different silica contents.

In contrast, this trend changed when the compressed silica composites exhibit a shifted G^+ peak to lower Raman shift values as shown in Fig. 6. The G^+ peak position seems to be independent of the w.t.% of 3 µm silica as the size of CNT bundles is various times smaller than the silica particles making it independent of the silica w.t.%.

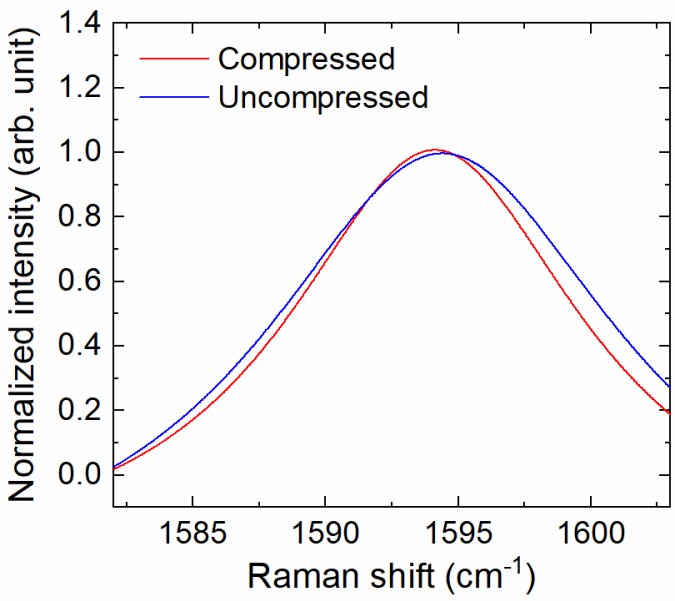

Figure 6. Raman spectra showing the G^+ peak positions of CNT-PDMS composites with 3 µm silica particles embedded Compressed and Uncompressed

The shift in G+ peak position in the Raman spectra after compression can result from longitudinal tensile strain on CNTs due to CNT compression by the silica microparticles. [36] This is rarely observed in CNT-polymer composites without additional solid microparticles.

4.2. Thermoelectric Transport Properties

Fig. 7 shows the measured Seebeck coefficients of the composites as a function of silica content before and after compression, along with theoretical fitting. The method used for sample compression is discussed in Supporting Information (Section 6). Sample Compression. The values obtained from the experiment are all positive, as shown in the figure, indicating unintentional p-type doping by oxidation in air. In both cases before and after compression, the Seebeck coefficient slightly decreased initially when a 10% silica MPs were added to CNT-PDMS composites. The initial small drop in Seebeck coefficient can be attributed to the disrupted CNT networks with addition of silica MPs, where the excluded volume effect was relatively too small to enhance the property.

From 10 % to 40 % silica, the Seebeck coefficient steadily increased with increasing silica content. We employed the Landauer formalism for the junction tunneling transport between CNTs to

explain this trend. Here, we used the average junction distance as a sole fitting parameter for both data before and after compression. We used steadily decreasing junction distance with increasing silica content up to 40 % to fit the experimental Seebeck coefficients for both before and after compression samples, which produced reasonable fitting for both before and after compression as shown in Fig. 7(a). Fig. 7(b) shows the average junction distance values used for the best curve fits as a function of silica content. Reduction of the average junction distance from ~ 11.5 to ~ 10 Å is obtained from the fitting for the as-synthesized samples before compression from 0 to 40 % silica. Further reduction of junction distance down to ~ 7 Å has been possible with sample compression as denser CNT networks can be created due to compaction.

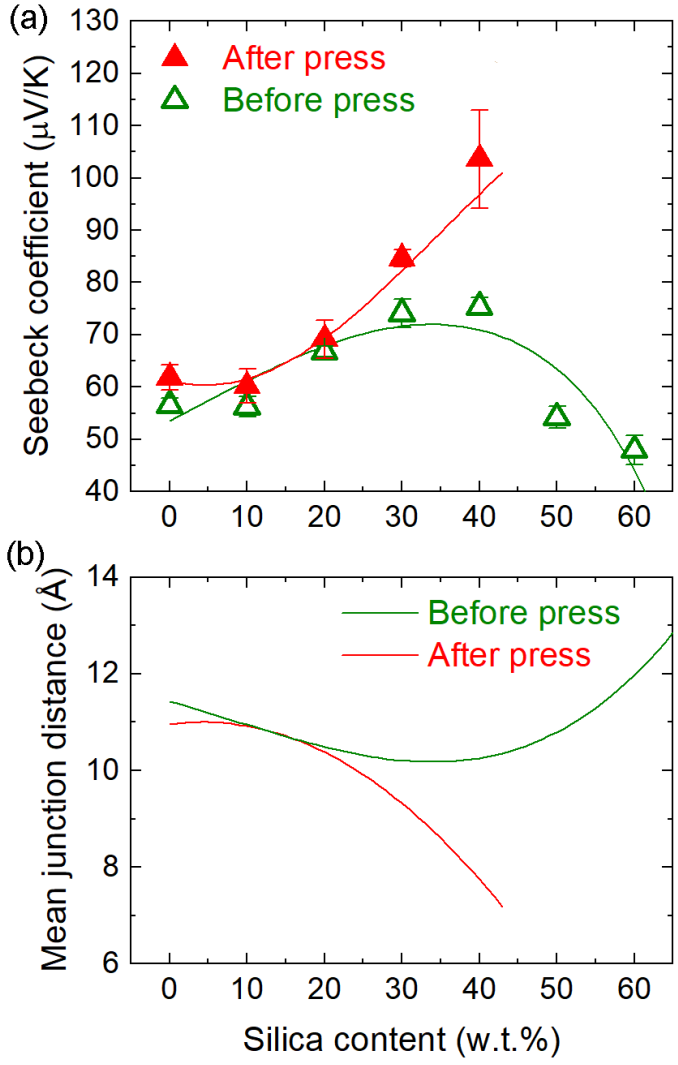

Figure 7. (a) Seebeck coefficient of SWCNT-silica MP-PDMS composites as a function of silica content (w.t.%) for 3 μm particle size before and after compression. The content of SWCNT was

fixed at 10 w.t.%, and PDMS content varied accordingly. Symbols are experimental data and curves are theoretical fitting. (b) Mean junction distances used in the theoretical fitting as a function of silica content. Up to 40 % silica, the junction distance is reduced with increasing silica content, which results in the increase in Seebeck coefficient. Beyond 40 %, due to the much-reduced PDMS content, the effective network enhancement by excluded volume was mitigated, resulting in the Seebeck coefficient reduction in the uncompressed samples.

Beyond 40 % silica, the decrease in Seebeck coefficient is observed as shown in Fig. 7(a) for uncompressed samples, which can be attributed to the increased material inhomogeneity due to the reduction of PDMS content as a binder, and more disruptive CNT networks with excess microparticles. As silica content increases, PDMS content was reduced accordingly. CNTs can still be bound well onto the surface of silica particles with less PDMS binder, but the hair-like inter-particle bridges made of PDMS-coated CNT bundles become apparently thinner and less observed due to the less amount of PDMS available as clearly seen in the SEM images in Fig. 3. We believe that these bridges play a crucial role in connecting the sub-networks of CNTs on individual particles to create larger-scale conduction pathways from end to end of the sample. Increased silica content above 40 % and the accordingly reduced PDMS content seem to have made these inter-particle connections poorer, resulting in the reduction in the Seebeck coefficient. We model this behavior by correlating the increased standard deviation of junction distance distribution linearly with the increase in the mean value. Note that samples with high silica contents above 40 % were relatively fragile due to the reduced PDMS content. These samples were damaged after compression; hence, the properties could not be measured.

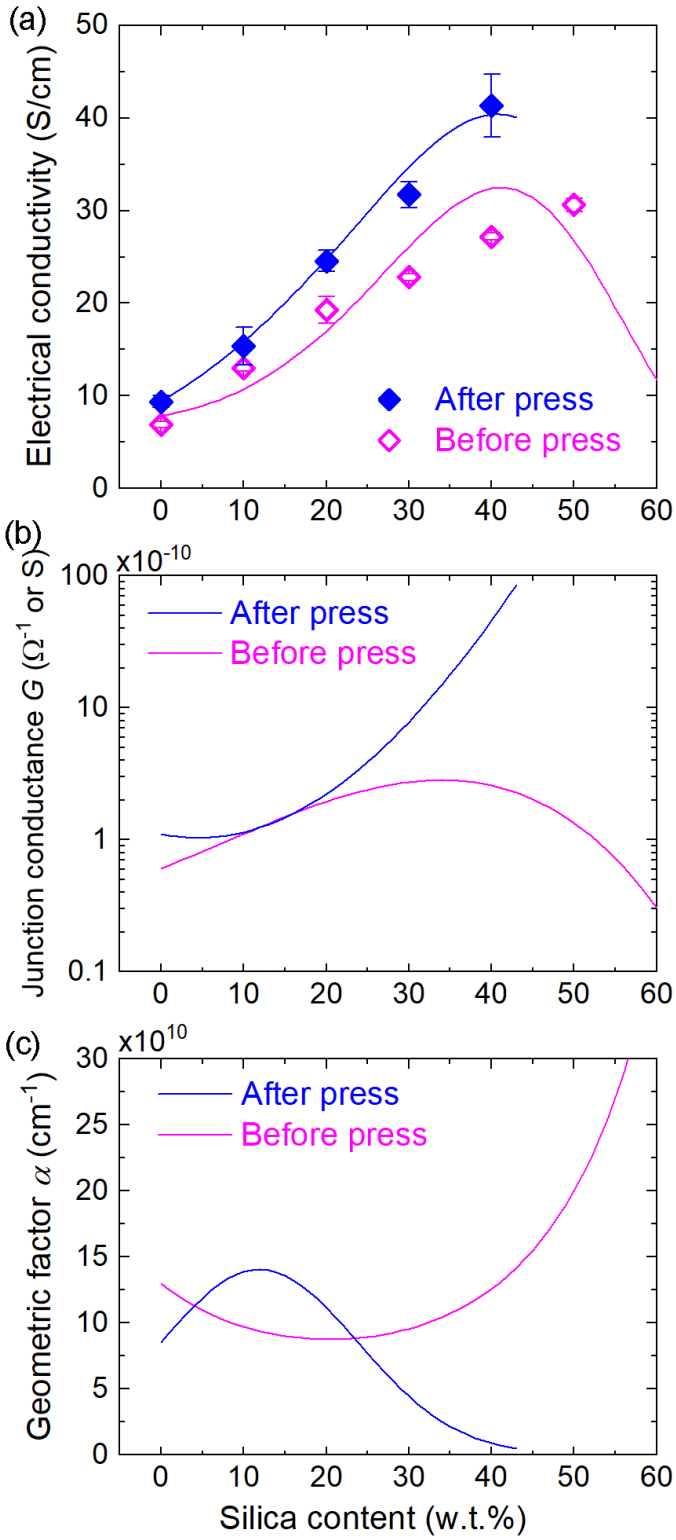

Figure 8. (a) Electrical conductivity of SWCNT-silica MP-PDMS composites as a function of silica w.t.% for 3 μm particle size before and after compression. The content of SWCNT was fixed at 10 w.t.%, and PDMS content varied accordingly, i.e., decreasing PDMS w.t.% with increasing silica content. Symbols are experimental data and curves are theoretical fitting. (b)

Junction conductance G calculated based on the theoretical fitting of the Seebeck coefficient shown in Fig. 7. (c) Geometric factor α as a function of silica content obtained from the fitting of the experimental electrical conductivity in (a) with the calculated junction conductance in (b) using Eq. (10).

Fig. 8 shows the electrical conductivity of the same set of samples as a function of silica content. The electrical conductivity also steadily increases with increasing silica content as the Seebeck coefficient does for both before and after compression. A gigantic 3-fold increase in the electrical conductivity was obtained by the inclusion of silica MPs at 40 % and total more than 4-fold increase after compression compared to that of the uncompressed, non-silica sample.

Fig. 8(b) and (c) show, respectively, the junction conductance and the geometric factor used to fit the experimental electrical conductivity as a function of silica content. As the junction distance decreases with increasing silica content, the junction conductance is enhanced, which is the main cause of the electrical conductivity enhancement. The geometric factor, however, decreases initially at low silica contents for uncompressed samples, but slows down in the decrease and eventually increases with increasing silica content above 20 ~ 30 % silica. We believe this is possible due to the re-organization of CNT networks. Initially, CNTs are re-organized as the silica MPs are added and create excluded volume, which can make existing channels partially merged instead of making new ones, resulting in fewer number of channels at low silica contents. As silica is added more and more, better-connected CNT networks, particularly with bundle bridges between sub-networks on particles, can be created, so that more parallel conduction channels are effectively created to increase m, and thus α.

As shown in Fig. 8(a), the compression effect led to an additional increase, approximately 40 %, in the electrical conductivity from that of uncompressed samples at high silica contents, 30 and 40 w.t.%. This enhancement largely comes from the further reduction in the junction distance by compression, i.e., G increased by compression. At the same time, the geometric factor is also increased particularly at low silica content by compression, which indicates the improvement in the CNT network alignment. Since the samples were pressed down vertically, CNTs could be better aligned in the horizontal direction, which is the transport direction for these in-plane measurements. After 20 ~ 30 % silica, however, the geometric factor after compression becomes smaller than that before compression, which can be attributed to the thinning down or even disconnection of CNT bundle bridges that were connecting sub-networks on silica particles due to

the tensile strain created by compression, resulting in the reduction of the number of parallel channels per cross-sectional area despite the reduced sample thickness after compression. We noticed that the samples were broken by compression at high silica contents above 40 %. It seems that the disruption of CNT networks has already started at lower silica contents, and steadily reduced the geometric factor down to zero with increasing silica content beyond 40 %. It should also be noted that irrespective of the silica size, the electrical conductivity values were somewhat similar considering the cases of either before compression or after compression. See Supporting Information (Section 5). This can be due to the fact that the density of conduction paths created by the excluded volume are similar for both 1 and 3 μm particle size.

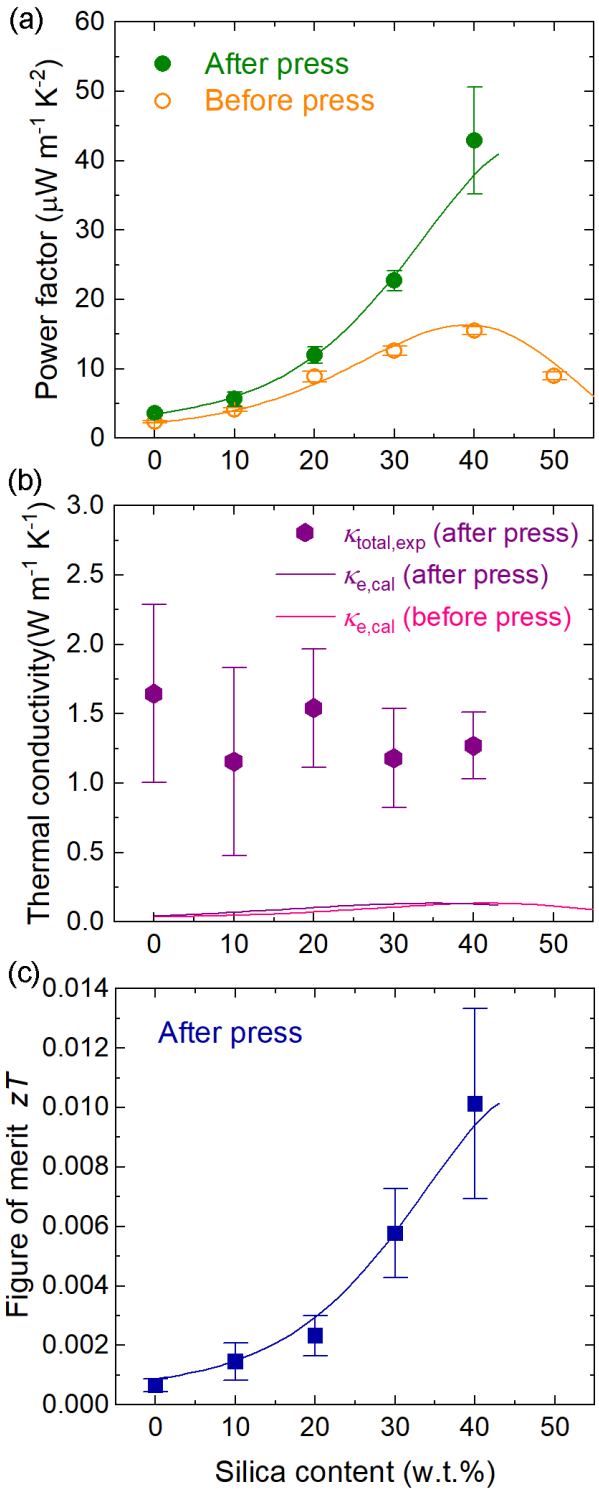

Figure 9. (a) Power factor, (b) thermal conductivity, and (c) figure of merit *zT* of SWCNT-silica MP-PDMS composites as a function of silica w.t.% with 3 μm diameter. Power factor was obtained for both compressed and uncompressed samples. Thermal conductivity was measured, and thus *zT* was obtained, only for compressed samples. The content of SWCNTs was fixed at 10 w.t.%, and PDMS content varied accordingly. Symbols are experimental data and curves are

theoretical fitting. In (b), the theoretical calculations are only electronic thermal conductivities.

As shown in Fig. 9(a), the addition of silica particles up to 40 % to the CNT-PDMS composite dramatically boosted the power factor. The maximum power factor achieved for 3 μm silica particles co-embedded in the CNT-PDMS composite are 15.5 $\mu W/mK^2$ before compression and 42. 9 $\mu W/mK^2$ after compression, which are more than 6-fold and 18-fold increases, respectively, from that of the uncompressed, no-silica sample (2.3 $\mu W/mK^2$). Beyond 40 w.t.% silica, the electrical conductivity slightly increases while Seebeck coefficient decreases quite a lot, resulting in the decrease of power factor.

Fig. 9(b) shows the thermal conductivity of the CNT-silica-PDMS composites measured by the Raman scattering technique. The thermal conductivity is roughly constant ~ 1.2 W/mK, irrespective of silica content. The calculated electronic thermal conductivity is found to be increasing with increasing silica content, but the maximum values are only ~ 0.13 W/mK, which is an order of magnitude smaller than the total thermal conductivity. This indicates that the lattice thermal conductivity is dominant over the electronic one in determining total thermal conductivity, which is consistent with previous reports [6,7]. Fig. 9(c) shows the figure of merit zT of the composites as a function of increasing silica content. The figure of merit shows a steady increase with a maximum value of 0.01 at 40 % silica for compressed samples. This value is still much lower than those of the state-of-the-art inorganic TE materials having $zT \sim 1$. It is noteworthy, however, that our approach takes into account the use of organic materials with several advantages such as low cost, nontoxic, biocompatible and environmentally friendly materials. Also, the zT value was obtained without any chemical treatment or high-energy processing for CNTs and only 10 w.t.% CNTs were used to realize the maximum zT value only through modification of CNT networks.

4.3. Bending Tests

The mechanical flexibility of the obtained compressed CNT-PDMS composite samples was characterized by radius-dependence conductivity measurement with silica content = 0, 10% and 40%. As shown in Fig. 10, the results show that the developed CNT-PDMS composites have great mechanical flexibility and stability with a maximum of ~4% reduction in electrical conductivity at

bending radius of 10 mm. The results are reproducible as the samples are highly elastic even after the sample compression.

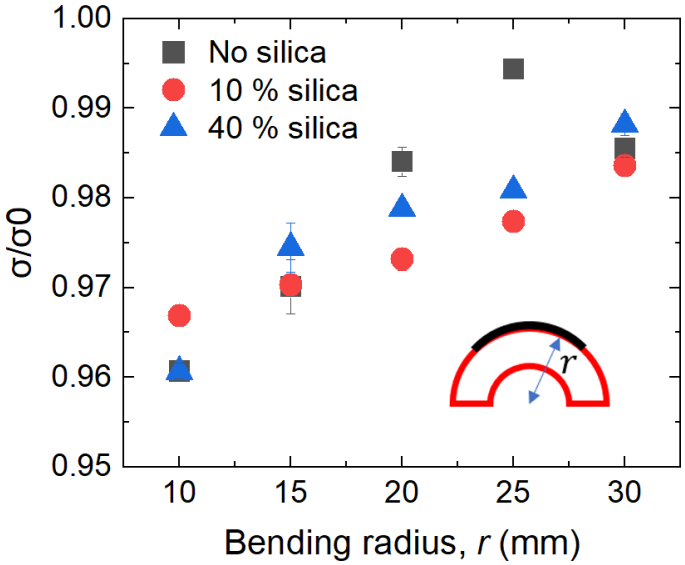

Figure 10. Bending radius-dependent electrical conductivity for CNT-silica-PDMS composites after compression for silica size = 3 μm and silica contents, 0, 10 and 40 w.t.%.

5. Conclusions

In short, we have demonstrated the creation of excluded volume by introducing silica microparticles into the CNT-PDMS composites to modify the CNT networks to enhance thermoelectric properties. Combined with the synergistic effect of sample compression enabled by the soft polymer matrix, this excluded volume method is valuable and highly effective in boosting the power factor without chemical treatments or CNT doping. In many cases, the power factors of various polymer-based hybrid composites were improved by increasing the electrical conductivity with little to no increase in the Seebeck coefficient with extensive doping. Our excluded volume method demonstrated a simultaneous increase in both electrical conductivity and Seebeck coefficient to drastically increase the power factor by more than a factor of 6, and an additional 3-fold increase was achieved by sample compression. We explain this power factor enhancement with reduced junction distance associated with the network modification by the excluded volume effect and sample compression within the framework of junction tunneling-dominant transport We demonstrated a zT value of 0.01. Further study might be necessary to improve the zT value with compositional optimization and additional doping. Also, future investigations are planned to

optimize the ratio of silica to CNTs, introducing supplementary reinforcing materials, or employing alternative compression or mechanical processing techniques to enhance the structural stability of the composites.

SUPPORTING INFORMATION

Composite synthesis and sample compression processes, materials and experimental methods, additional SEM images of composites, Raman spectroscopy analysis, additional TE property data with 1 μm silica particles, thickness data before and after compression, and Raman thermal mapping method

ACKNOWLEDGMENT

This material is based upon work supported by the National Science Foundation under Grants No. 1905571 and 1905037. V.S. and V.K.R.K. thank support from NIOSH through a grant #T42OH008432 from the Pilot Research Project Training Program of the University of Cincinnati (UC) Education and Research Center, NSF [grants IIP-2016484 and CBET-2028625], and the UC Collaborative Research Advancement Grant No. 1018371.

References

1. Bell, L. Cooling, Heating, Generating Power, and Recovering Waste Heat with Thermoelectric Systems. Science, **2008**, 321, 1457.
2. Hewawasam, L.S.; Jayasena, A.S.; Afnan, M.M.M.; Ranasinghe, R.A.C.P.; Wijewardane, M.A. Waste Heat Recovery from Thermo-Electric Generators (TEGs). Energy Reports **2020**, 6, 474–479.
3. Bahk, J.-H.; Fang, H.; Yazawa, K.; Shakouri, A. Flexible Thermoelectric Materials and Device Optimization for Wearable Energy Harvesting. J. Mater. Chem. C **2015**, 3, 10362-10374.
4. Heremans, J.P.; Dresselhaus, M.S.; Bell, L.E.; Morelli, D.T. When Thermoelectrics Reached the Nanoscale. Nat. Nanotech. **2013,** 8, 471.
5. Hsieh, Y.Y.; Zhang, Y.; Zhang, L.; Fang, Y.; Kanakaraaj, S.N.; Bahk, J.H.; Shanov, V. High Thermoelectric Power-Factor Composites Based on Flexible Three-Dimensional Graphene and Polyaniline. Nanoscale **2019**, 11, 6552–6560.
6. Blackburn, J.L.; Ferguson, A.J.; Cho, C.; Grunlan, J.C. Carbon-Nanotube-Based Thermoelectric Materials and Devices. Advanced Materials **2018**, 30, 1704386.
7. Avery, A.D.; Zhou, B. H.; Lee, J.; Lee, E.-S.; Miller, E.; Ihly, R.; Wesenberg, D.; Mistry, K.; Guillot, S.; Zink, B.; Kim, Y.-H.; Blackburn J.L.; Ferguson, A.J. Tailored

Semiconducting Carbon Nanotube Networks with Enhanced Thermoelectric Properties. Nat. Energy **2016**, 1, 16033.
8. Park, K.; Lee, T.; Ko, Y.; Cho, Y.; Park C.; Kim, H. High-Performance Thermoelectric Fabric Based on a Stitched Carbon Nanotube Fiber. ACS Appl. Mater. Interfaces **2021**, 13, 6257-6264.
9. Hicks, I.D.; Dresselhaus, M.S. Thermoelectric Figure of Merit of a One-Dimensional Conductor. **1993**, 47, 16631.
10. Balandin, A. A. Thermal Properties of Graphene and Nanostructured Carbon Materials. Nat. Mater. **2011**, 10, 569.
11. Small, J.P.; Perez, K.M.; Kim, P. Modulation of Thermoelectric Power of Individual Carbon Nanotubes. Phys. Rev. Lett. **2003**, 91, 256801.
12. Yu, C.; Shi, L.; Yao, Z.; Li, D.; Majumdar, A. Thermal Conductance and Thermopower of an Individual Single-Wall Carbon Nanotube. Nano Lett. **2005**, 5, 1842.
13. Prabhakar, R.; Hossain, S.; Zheng, W.; Athikam, P.K.; Zhang, Y.; Hsieh, Y.-Y.; Skafidas, E.; Wu, Y.; Shanov, V.; Bahk, J.-H. Tunneling-Limited Thermoelectric Transport in Carbon Nanotube Networks Embedded in Poly(dimethylsiloxane) Elastomer. ACS Appl. Energy Mater. **2019**, 2, 2419.
14. Yu, C.; Choi, K.; Yin, L.; Grunlan, J.C. Light-Weight Flexible Carbon Nanotube Based Organic Composites with Large Thermoelectric Power Factors. ACS Nano **2011**, 5, 7885.
15. Yu, C.; Kim, Y.S.; Kim, D.; Grunlan, J.C. Thermoelectric Behavior of Segregated-Network Polymer Nanocomposites. Nano Lett. **2008**, 8, 4428–4432.
16. Tang, J.; Chen, Y.; McCuskey, S.R.; Chen, L.; Bazan, G.C.; Liang, Z. Recent Advances in N-Type Thermoelectric Nanocomposites. Adv Electron Mater **2019**, 5, 1800943.
17. Nakai, Y.; Honda, K.; Yanagi, K.; Kataura, H.; Kato, T.; Yamamoto, T.; Maniwa, Y. Giant Seebeck Coefficient in Semiconducting Single-Wall Carbon Nanotube Film. Applied Physics Express **2014**, 7, 25103
18. Nonoguchi, Y.; Ohashi, K.; Kanazawa, R.; Ashiba, K.; Hata, K.; Nakagawa, T.; Adachi, C.; Tanase, T.; Kawai, T. Systematic Conversion of Single Walled Carbon Nanotubes into N-Type Thermoelectric Materials by Molecular Dopants. Scientific Reports, **2013**, 3, 3344.
19. Macleod, B.A.; Stanton, N.J.; Gould, I.E.; Wesenberg, D.; Ihly, R.; Owczarczyk, Z.R.; Hurst, K.E.; Fewox, C.S.; Folmar, C.N.; Hughes, K.H.; et al. Large N-and p-Type Thermoelectric Power Factors from Doped Semiconducting Single-Walled Carbon Nanotube Thin Films. Energy Environ. Sci. **2017**, 10, 2168.
20. Statz, M.; Schneider, S.; Berger, F.J.; Lai, L.; Wood, W.A.; Abdi-Jalebi, M.; Leingang, S.; Himmel, H.-J.; Zaumseil, J. and Sirringhaus, H. Charge and Thermoelectric Transport in Polymer-Sorted Semiconducting Single-Walled Carbon Nanotube Networks. ACS Nano **2020,** 14, 15552.
21. Prasher, R.S. Hu, X.J.; Chalopin, Y.; Mingo, N.; Lofgreen, K.; Volz, S.; Cleri, F.; Keblinski, P. Turning Carbon Nanotubes from Exceptional Heat Conductors into Insulators. Phys. Rev. Lett. **2009**, 102, 105901.

22. Chalopin, Y.; Volz, S.; Mingo, N. Upper Bound to the Thermal Conductivity of Carbon Nanotube Pellets. Journal of Applied Physics, **2009**, 105, 084301.
23. Evans, W.J.; Shen, M.; Keblinski, P. Inter-tube Thermal Conductance in Carbon Nanotubes Arrays and Bundles: Effects of Contact Area and Pressure. Appl. Phys. Lett. **2012**, 100, 261908.
24. Yao, Q.; Wang, Q.; Wang, L.; Chen, L. Abnormally Enhanced Thermoelectric Transport Properties of SWNT/PANI Hybrid Films by the Strengthened PANI Molecular Ordering. Energy Environ. Sci. **2014**, 7, 3801.
25. Liang, L. Chen, G.; Guo, C.-Y. Enhanced Thermoelectric Performance by Self-assembled Layered Morphology of Polypyrrole Nanowire/Single-Walled Carbon Nanotube Composites. Composites Science and Technology, **2016**, 129, 130.
26. Park, S.H.; Hwang, J.; Park, G.S.; Ha, J.H.; Zhang, M.; Kim, D.; Yun, D.J.; Lee, S.; Lee, S.H. Modeling the Electrical Resistivity of Polymer Composites with Segregated Structures. Nat Commun. **2019**, 10, 2537
27. Palza, H.; Garzón, C.; Arias, O. Modifying the Electrical Behaviour of Polypropylene/Carbon Nanotube Composites by Adding a Second Nanoparticle and by Annealing Processes. Express Polym. Lett. **2012**, 6, 639–646.
28. Palza, H.; Reznik, B.; Wilhelm, M.; Arias, O.; Vargas, A. Electrical, Thermal, and Mechanical Characterization of Poly(Propylene)/Carbon Nanotube/Clay Hybrid Composite Materials. Macromol. Mater. Eng. **2012**, 297, 474-480.
29. Diekmann, A.; Omelan, M.C. v; Giese, U.; Bielí, D.M. Influence of Carbon Nanotube-Pretreatment on the Properties of Polydimethylsiloxane/Carbon Nanotube-Nanocomposites. Polymers **2021**, 13, 1355.
30. Liu, J.; Zong, G.; He, L.; Zhang, Y.; Liu, C.; Wang, L.; Effects of Fumed and Mesoporous Silica Nanoparticles on the Properties of Sylgard 184 Polydimethylsiloxane. Micromachines **2015**, 6(7), 855-864.
31. Isaiev, M.; Didukh, O.; Nychyporuk, T.; Timoshenko, V.; Lysenko, V. Anisotropic Heat Conduction in Silicon Nanowire Network Revealed by Raman Scattering. Appl. Phys. Lett. **2017**, 110, 011908.
32. Kim, R.; Datta, S.; Lundstrom, M. S. Influence of Dimensionality on Thermoelectric Device Performance. J. Appl. Phys. **2009**, 105, 034506.
33. Hansen, K.; Brandbyge, M. Current-Voltage Relation for Thin Tunnel Barriers: Parabolic Barrier Model. J. Appl. Phys. **2004**, 95, 3582.
34. Wertheim, G.K.; Butler, M. A.; West, K. W.; Buchanan, D. N. E. Determination of the Gaussian and Lorentzian Content of Experimental Line Shapes. Rev. Sci. Instrum. **1974**, 45, 1369-1371.
35. Kondapalli, V. K. R.; He, X.; Khosravifar, M.; Khodabakhsh, S.; Collins, B.; Yarmolenko, S.; Paz Puente, A.; Shanov, V. CVD Synthesis of 3D-Shaped 3D Graphene Using a 3D-Printed Nickel−PLGA Catalyst Precursor. ACS Omega **2021**, 6, 29009.
36. Liu, Z.; Zhang, J.; Gao, B. Raman Spectroscopy of Strained Single-walled Carbon Nanotubes. Chem. Commun. **2009**, 6902-6918.